# Electronic Supplementary Informations: Influence of proliferation on the motions of epithelial monolayers invading adherent strips

Estelle Gauquelin,[a] Sham Tlili,[c] Cyprien Gay,[b] Grégoire Peyret,[a] René-Marc Mège,[a] Marc A. Fardin*[a] and Benoît Ladoux*[a,c]

March 7, 2019

## 1 Height of the monolayer.

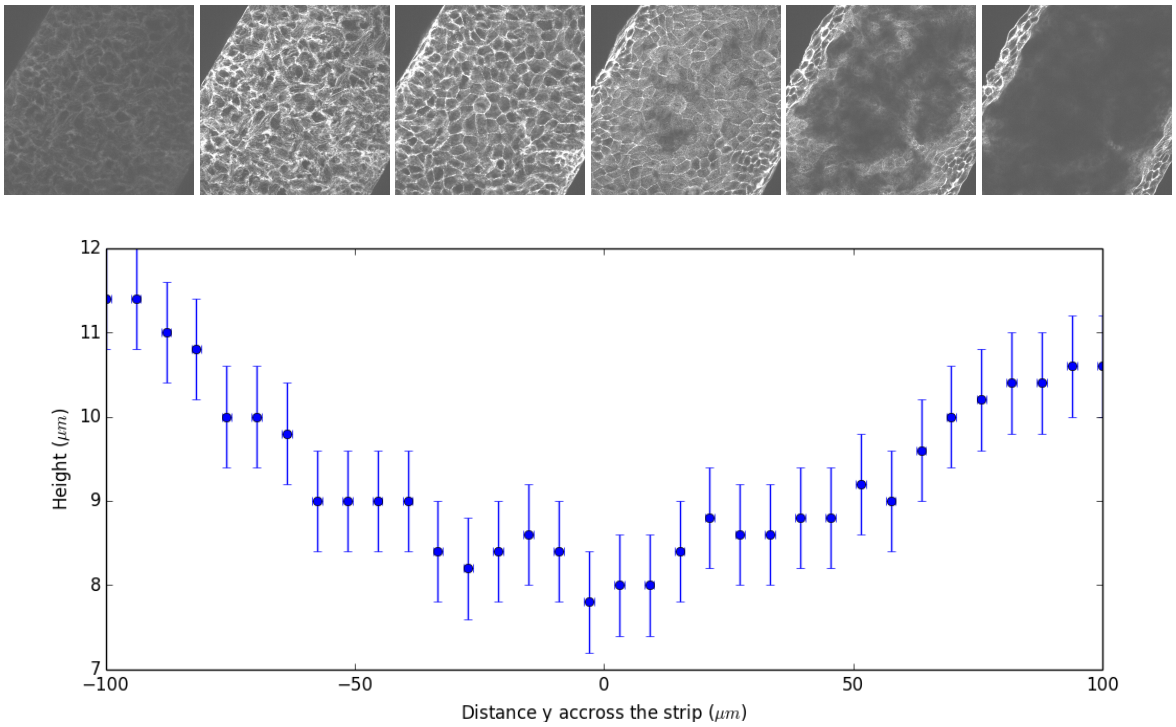


Figure 1: (top) Confocal slices: at the substratum, and every $2\mu$m away from it. The scale is given by the width of the strip, which is $200\mu$m (from top to bottom, left to right). (bottom) Average height of the epithelium as a function of the distance $y$ across the strip.

In the article, we considered that the height of the monolayer was $H = 9 \pm 1$ $\mu$m. This value is based on measurements done by confocal microscopy. Cells are stained with PBD-YFP (p21-binding domain) making their frontiers apparent. As shown in Fig. 1, confocal slices at various heights above the substratum reveal the height of the monolayer. We found that this height was about 30% lower in the middle of the epithelium ($y = 0$) than on the sides ($y = \pm 100\mu$m).

[a] *Institut Jacques Monod (IJM), Université Denis Diderot - Paris 7, CNRS UMR 7592, Paris 72505, France.*
[b] *Laboratoire Matière et Systèmes Complexes, Université Denis Diderot - Paris 7, CNRS UMR 7057, Paris 72505, France.*
[c] *Mechanobiology Institute, National University of Singapore, 5A Engineering Drive 1, Singapore 117411.*
* Corresponding authors: marc-antoine.fardin@ijm.fr and benoit.ladoux@ijm.fr

## 2 Gradient of velocity in the flow direction.

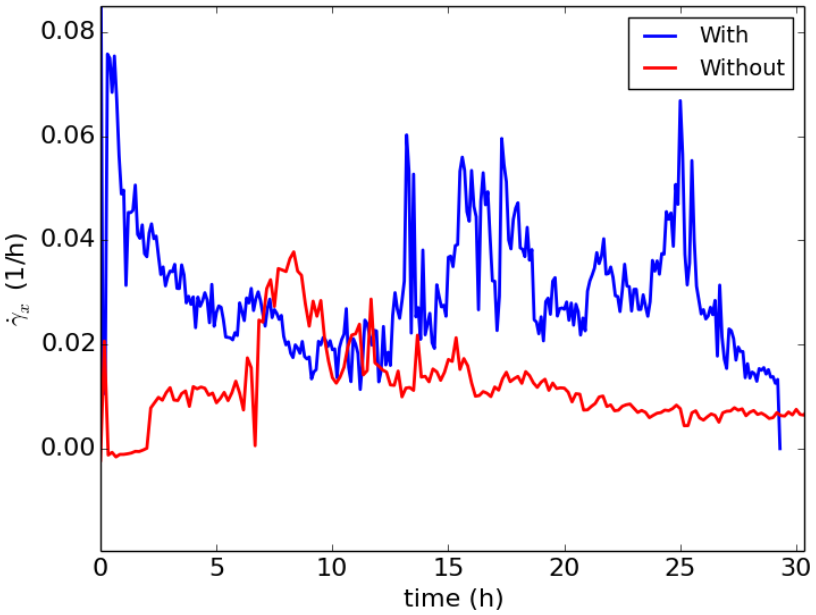


Figure 2: Two examples of the evolution of the velocity gradient $\dot{\gamma}_x(t)$, with or without divisions.

As discussed in the article, with and without divisions the monolayer flow is restricted to a band behind the advancing front. Velocity is maximum at the front and decreases roughly linearly toward the bulk where motion virtually stop. The extent of the flowing band, $\xi(t)$, increases during the experiment, whereas the velocity of the front stay roughly constant. Fitting the velocity profile in the direction of the strip by a linear relation yields a measure of the evolution of $\xi(t)$ and of the gradient $\dot{\gamma}_x = \frac{\partial u}{\partial x} \simeq U/\xi$. Fig. 2 gives two examples of the evolution of $\dot{\gamma}_x$ corresponding to the two examples of $\xi(t)$ given in the article.

## 3 Proliferation and cell size.

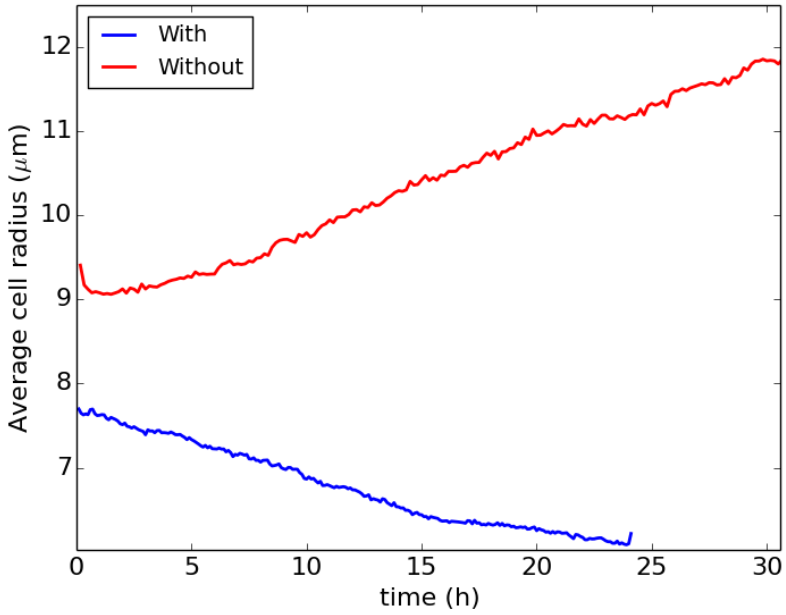


Figure 3: Two examples of the evolution of the mean radius $\bar{R}(t)$, with or without divisions.

As discussed in the article, the mean cell radius $\bar{R}(t)$–averaged over the entire epithelium–can be computed directly from the extent of the monolayer, $L(t)$ and the number of cells, $N(t)$:

$$\bar{R}(t) = \sqrt{\frac{S(t)}{\pi N(t)}} = \sqrt{\frac{wL(t)}{\pi N(t)}} \tag{1}$$

Two examples representative of the conditions with or without divisions are given in Fig. 3, where the mean radius is seen to increase in the absence of divisions, and to decrease in the presence of divisions.

Since both the extent of the monolayer, $L(t)$, and the number of cells, $N(t)$, increase linearly for the duration of the experiments, the mean cell radius can be expressed using:

$$\bar{R}(t) \simeq \sqrt{\frac{w(L_0+Ut)}{\pi N_0(1+Kt)}} = \bar{R}_0\sqrt{\frac{1+\tilde{K}t}{1+Kt}} \tag{2}$$

where $K$ and $\tilde{K} = U/L_0$ represent respectively the rate of proliferation and of geometrical expansion. The distributions of $K$ with and without proliferation are given in the article. The associated distributions of $\tilde{K}$ are given in Fig. 4a.

In the experiments described in the article, we are always at 'short time' in comparison to $K^{-1}$ and $\tilde{K}^{-1}$, such that the expression for the mean radius $\bar{R}(t)$ can be simplified further:

$$\bar{R}(t) \simeq \bar{R}_0\left(1 + \frac{\tilde{K}-K}{2}t + \mathcal{O}(t^2)\right) \tag{3}$$

Whether or not the mean radius grows or decay then depends on the inequality between $K$ and $\tilde{K}$. The distributions of consolidated evolution rate of the mean radius, $\frac{\tilde{K}-K}{2}$, are given in Fig. 4b.

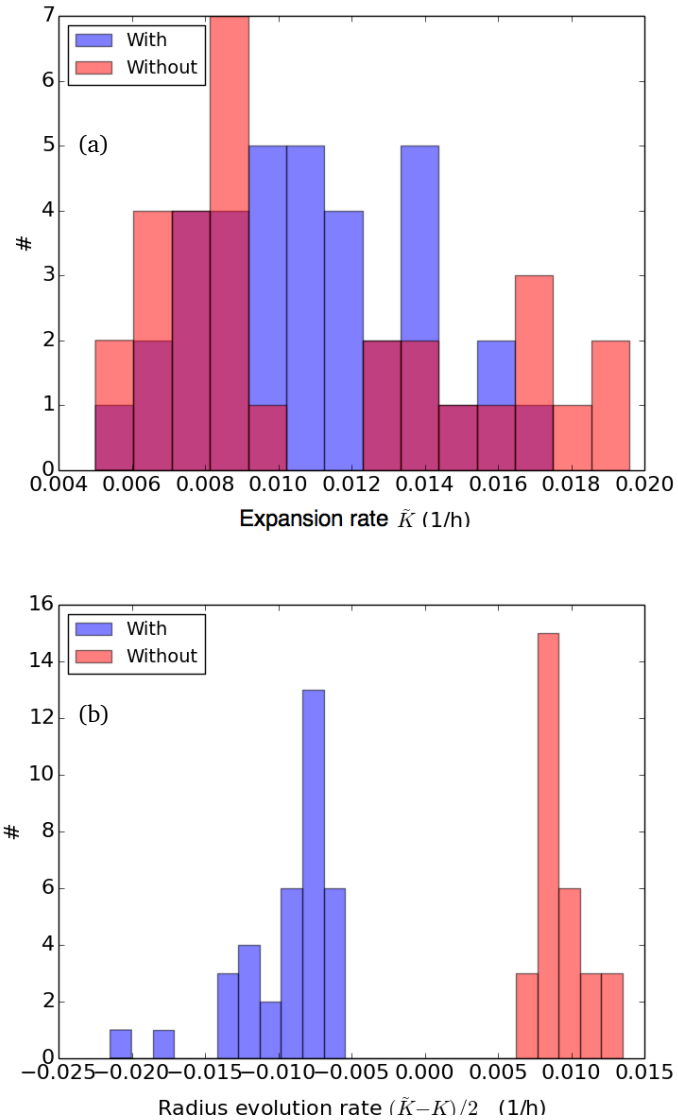


Figure 4: (a) Distributions of expansion rate $\tilde{K} = U/L_0$, with or without divisions. (b) Distributions of the mean radius evolution rate $\frac{\tilde{K}-K}{2}$, with or without divisions.

## 4 Velocity-radius relation.

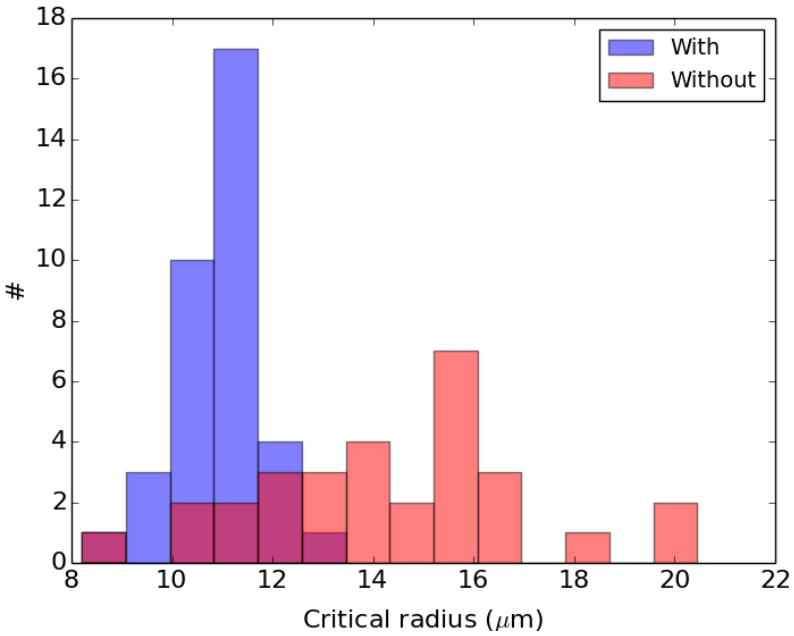


Figure 5: Distributions of critical radius $R_c$ with or without divisions.

### 4.1 piecewise velocity-radius relation

In the article, we chose a simple piecewise velocity-radius relation:

$$u(R) \simeq \begin{cases} 0 & \text{if } R \leq R_j \\ \dfrac{R-R_j}{\tau_v} & \text{if } R_j < R < R_c \\ \dfrac{R_c-R_j}{\tau_v} & \text{if } R \geq R_c \end{cases} \tag{4}$$

The distributions of jamming radius $R_j$ and time $\tau_v$ obtained by fitting the velocity-radius data for individual experiments with or without proliferation are given in the article. The corresponding distributions of critical radius $R_c$ are given in Fig. 5.

To compare more synthetically various forms of velocity-radius relations, the piecewise relation can be applied to the mean velocity-radius curves for all experiments with or without divisions. The best piecewise fits to the mean curves are given in in Fig. 6a. The parameters of the fits are:

| | With | Without |
|---|---|---|
| $R_j$ ($\mu$m) | 6.8 | 7.7 |
| $R_c$ ($\mu$m) | 12.3 | 14.2 |
| $\tau_v$ (min) | 13.3 | 28.3 |

In the article, we mentioned that the front speed $U$ is usually larger than the maximum velocity $\frac{R_c-R_j}{\tau_v}$ of the curve $u(R)$. Indeed, the maximum velocity of the curve incorporates values from large cells at the front as well as further behind, where velocities are smaller. Nevertheless, the two quantities remain in a linear relationship, as seen in Fig. 7a. If the radius of cells at the front is used of $R_c$, a similar linear relationship is found, as seen in Fig. 7b. Indeed, the critical radius and the radius of cells at the front are also in a linear relationship as seen in Fig. 7c.

### 4.2 Hyperbolic tangent velocity-radius relation

The piecewise relation is simple yet discontinuous. We study here a more continuous approach to the velocity-radius relation. Experimental data can be fitted to a hyperbolic tangent:

$$u(R) = \frac{u_m}{2}\left(\tanh\frac{R-R_0}{\Delta}+1\right) \tag{5}$$

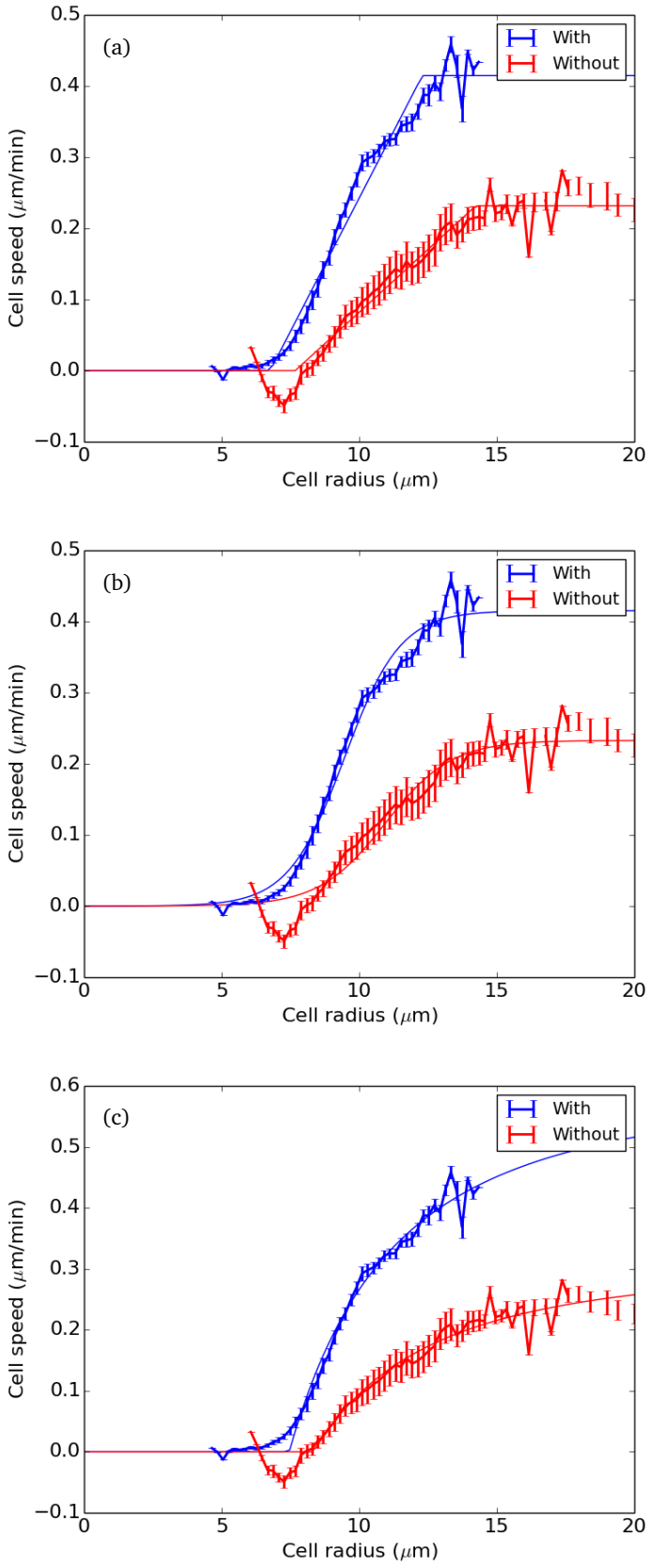


Figure 6: Best fits to the mean curves for all experiments with or without divisions, using (a) a piecewise linear function, (b) a hyperbolic tangent, (c) a Greenshields relation.

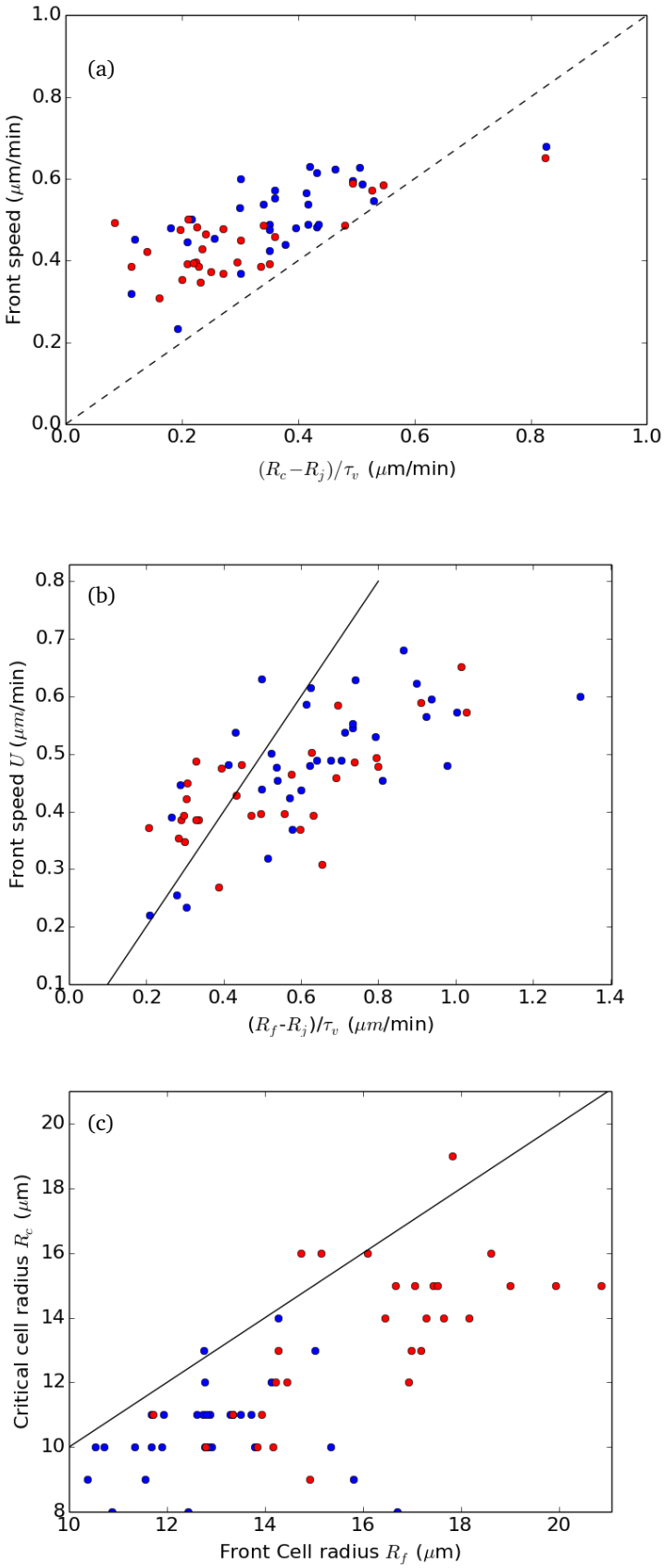


Figure 7: (a) Relationship between the front speed $U$ and the maximum of the radius-velocity curve $u(R)$. (b) Relationship between the speed computed from the radius of cells at the front and the front speed $U$. (c) Relationship between the critical radius and the radius of cells at the front. All lines draw the function $y = x$.

where $u_m$ is the maximum velocity for $R \gg R_0$, $R_0$ is the location of the maximum in slope of $u(R)$, and $\Delta$ is the spread of the hyperbolic tangent.

The best piecewise fits to the mean curves for all experiments with or without divisions are given in in Fig. 6b. The parameters of the fits are:

| | With | Without |
|---|---|---|
| $u_m$ ($\mu$m/min) | 0.4 | 0.2 |
| $R_0$ ($\mu$m) | 9.5 | 10.9 |
| $\Delta$ ($\mu$m) | 2.0 | 2.4 |

### 4.3 Greenshields velocity-radius relation

In the context of traffic flows, a velocity-density relation is often used. It is called the Greenshields relation and when expressed as a function of the mean radius it reads:

$$u(R) \simeq \begin{cases} 0 & \text{if } R \leq R_j \\ u_m\left(1 - \left(\frac{R_j}{R}\right)^2\right) & \text{if } R > R_j \end{cases} \tag{6}$$

The best piecewise fits to the mean curves for all experiments with or without divisions are given in in Fig. 6c. The parameters of the fits are:

| | With | Without |
|---|---|---|
| $u_m$ ($\mu$m/min) | 0.6 | 0.3 |
| $R_j$ ($\mu$m) | 7.4 | 8.3 |

## 5 Influence of the cytoskeleton.

As mentioned in the article, we tested the effect of actin polymerization on the motion of epithelia by adding the drug CK666 (100$\mu$M), a day after the onset of motion, and recorded the subsequent motion for an additional day (# = 30). In order to study the effect of CK666 on the waves as well as on the main flow, the studied cells were systematically treated with mitomycin, to be in non-proliferating conditions. The velocity of the front speed and the parameters of the velocity-radius relations were extracted systematically before and after the addition of CK666. The average velocity-radius curves before and after the addition of CK666 are given in Fig. 8. The jamming and critical radii are unchanged, but the coefficient of proportionality between speed and radius is, such that the maximum of the curve after the addition of the drug is substantially lower. This suggests that the front speed is also lower, as is indeed observed in the experiments. Distributions of $U$, $R_j$, $R_c$ and $\tau_v$ before and after are given in Fig. 9.

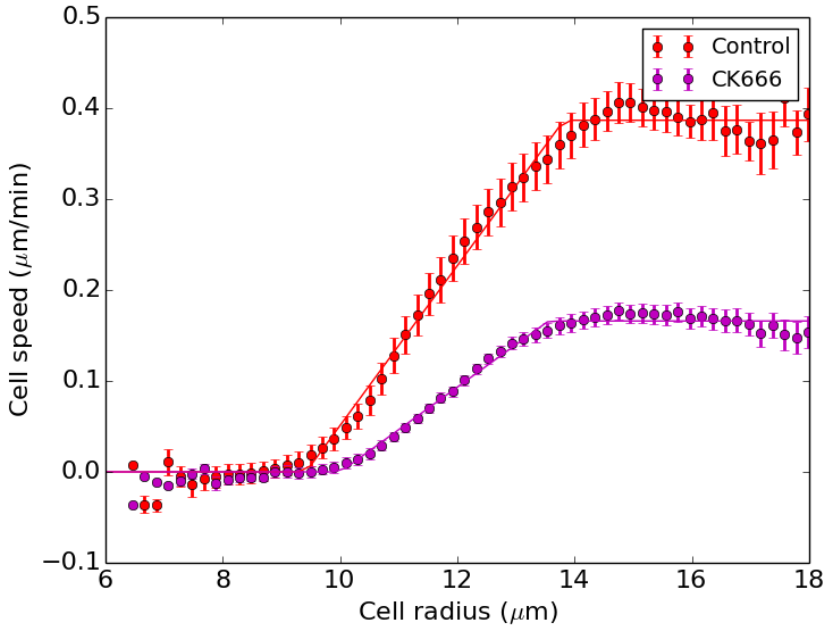


Figure 8: Velocity-radius curves before and after the addition of CK666 averaged over all experiments (# = 30).

Since cells in these experiments were in non-proliferating conditions, waves were present before the addition of CK666, with characteristics similar to the one reported in the article. After the addition of the drug, waves were still present, but we observed a substantial increase of the wave period $T_w$, and a decrease in their amplitude, as can be seen on the space-time diagram of the velocity in Fig. 10, and in Fig. 11.

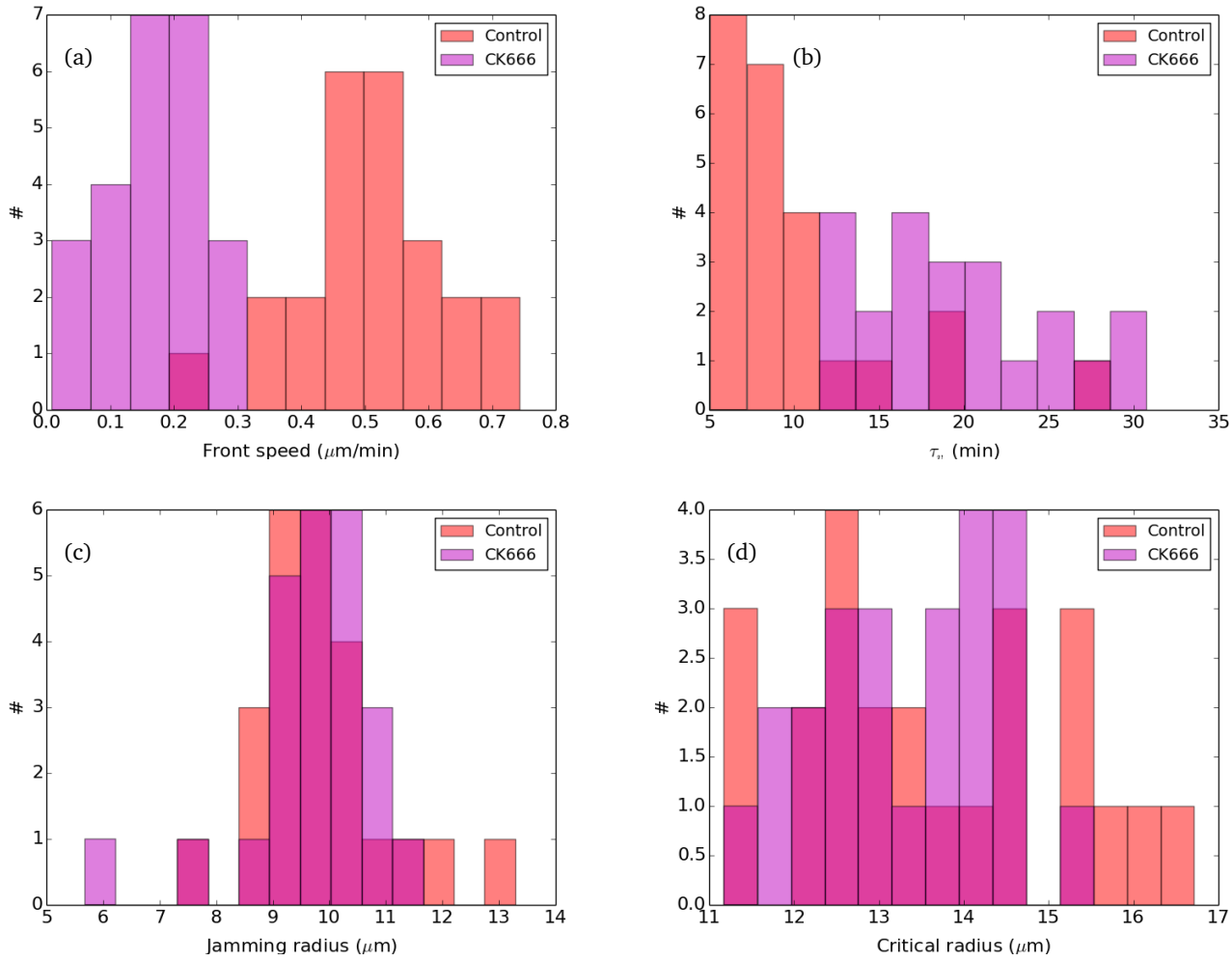


Figure 9: Distributions of main flow properties before and after the addition of CK666: (a) Front speed $U$, (b) Velocity-radius time $\tau_v$, (c) Jamming radius $R_j$, (d) Critical radius $R_c$.

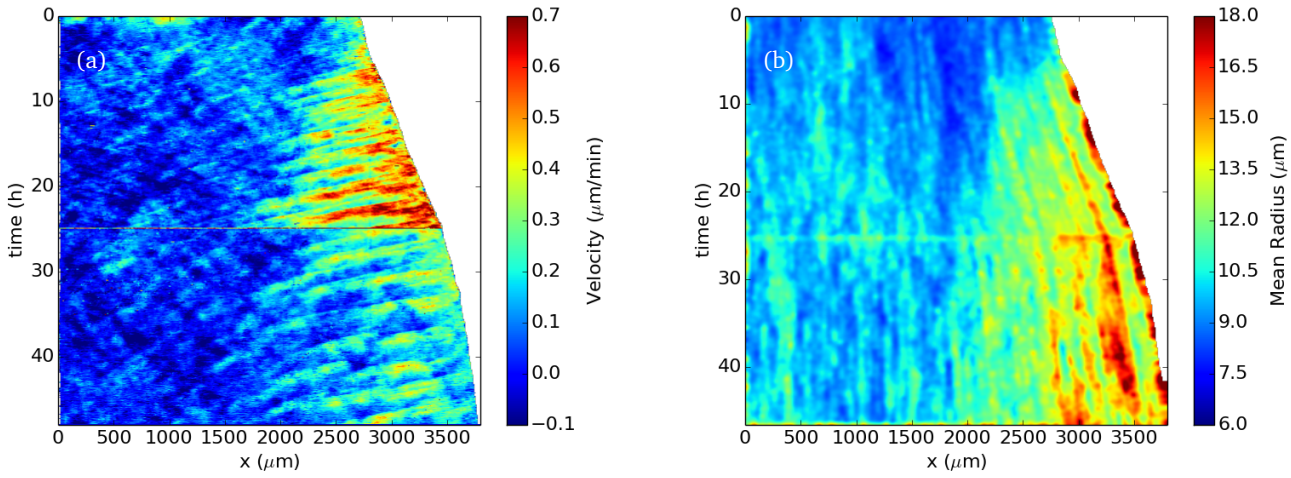


Figure 10: Velocity (a) and mean radius (b) space-time maps for a representative example of an experiments where CK666 is added 24 hours after the beginning of experiment in non-proliferating conditions. The instant were CK666 is added is visible by a short perturbation in the measurements of radii and velocities due to the transient blurring of the images.

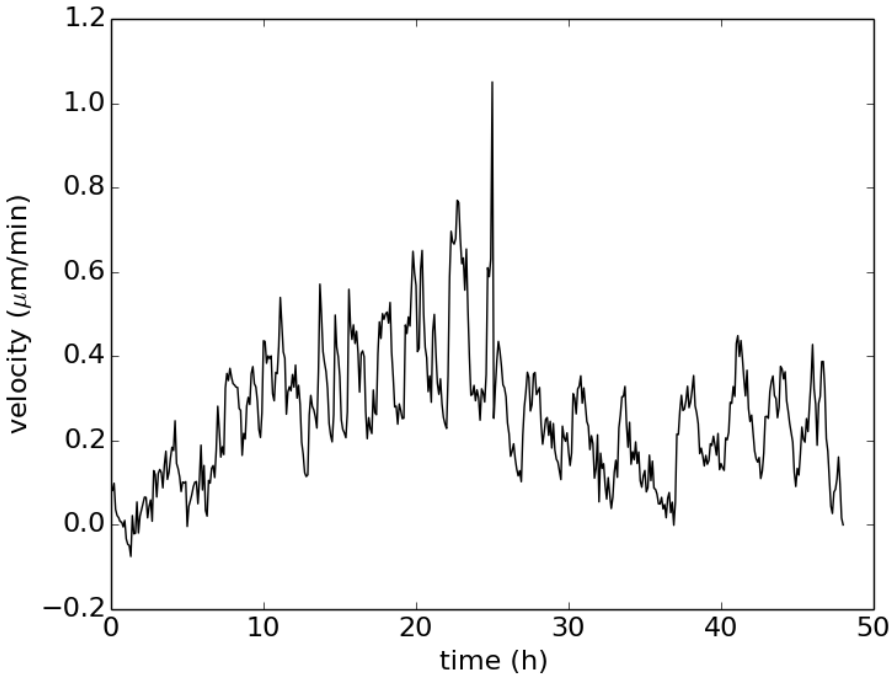


Figure 11: Velocity 500 $\mu$m behind the front for the example represented in Fig. 10a. A lengthening of the wave period is apparent.

## 6 Motion for low initial density.

The experiments discussed in detail in the article all have initial densities corresponding to an average initial radius of cells $\langle R_0 \rangle = 8.5 \pm 0.1$ $\mu$m, which is close to the jamming radius. Thus, the subsequent rarefaction of the epithelium near the front immediately leads to a motion driven by the proportionality between the cell radius and its speed. Nevertheless, since we know that this proportionality breaks down above a second critical radius $R_c$, we performed a few experiment at very low initial densities, to test if the subsequent dynamics was different in that case. For these experiment (# = 8), the initial number of cells is much smaller, with $\langle N_0 \rangle = 135 \pm 18$. Given how small this number is, the number of divisions is negligible over the course of the experiment, and we pulled together data with (# = 3) or without (# = 5) mitomycin C. The average cell radius in these experiments was very large, as can be seen in Fig. 12, with a mean initial value $\langle R_0 \rangle = 18.3 \pm 1.4$ $\mu$m, which is above the critical radius $R_c$, regardless of proliferation. Under such initial conditions, the mean front speed is $\langle U \rangle = 0.4 \pm 0.1$ min, comparable to the other experiments, but the proportionality between size and speed in the bulk broke down, as seen in Fig. 12 (b).

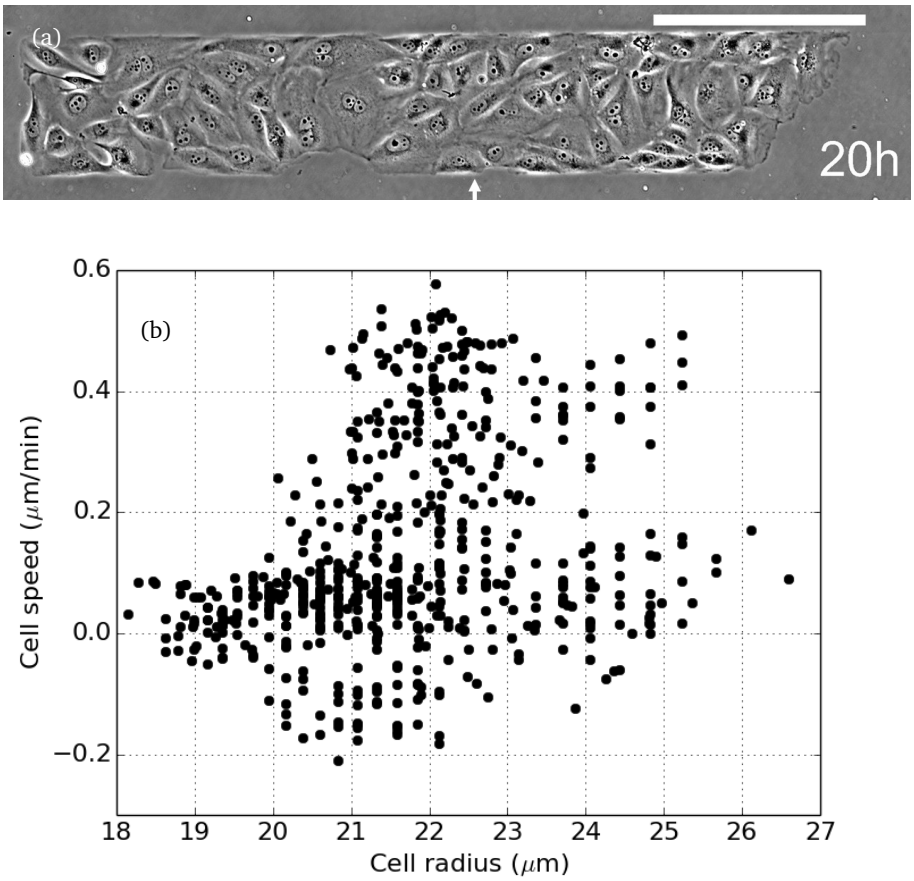


Figure 12: (a) Snapshot of the epithelium 20 hours after the beginning of an experiment with low initial cell density. The white arrow marks the initial location of the front. The scale bar is 250 $\mu$m. (b) Corresponding plot of the cell velocity versus cell density, showing the breakdown of the proportionality discussed in the article for higher initial densities.

## 7 Theory: Kinematic approach.

### 7.1 Amplitude of density waves

In the article we mentioned that we could not detect waves on the density data in our experiments. We here provide an explanation for such negative result. We start from the continuity equation:

$$\frac{\partial n}{\partial t} + \frac{\partial (un)}{\partial x} = Kn \tag{7}$$

We then introduce perturbations:

$$\begin{cases} n &= n_0 + \tilde{n} \exp i(qx - \omega t) \\ u &= u_0 + \tilde{u} \exp i(qx - \omega t) \end{cases} \tag{8}$$

The equation linearised for the perturbation (neglecting the quadratic term $\tilde{n}\tilde{u}$) is:

$$-i\omega \frac{\tilde{n}}{n_0} + iqu_0 \frac{\tilde{n}}{n_0} + iq\tilde{u} + \frac{\tilde{n}}{n_0}\frac{\partial u_0}{\partial x} + \frac{\tilde{u}}{n_0}\frac{\partial n_0}{\partial x} = K\frac{\tilde{n}}{n_0} \tag{9}$$

$$-i\frac{\omega}{qu_0}\frac{\tilde{n}}{n_0} + i\frac{\tilde{n}}{n_0} + i\frac{\tilde{u}}{u_0} + \frac{\tilde{n}}{n_0}\frac{1}{qu_0}\frac{\partial u_0}{\partial x} + \frac{\tilde{u}}{u_0}\frac{1}{qn_0}\frac{\partial n_0}{\partial x} = \frac{K}{qu_0}\frac{\tilde{n}}{n_0} \tag{10}$$

$$\Big(-i\frac{1}{Ma} + i + \frac{1}{qu_0}\frac{\partial u_0}{\partial x} - \frac{K}{qu_0}\Big)\frac{\tilde{n}}{n_0} = -\Big(i + \frac{1}{qn_0}\frac{\partial n_0}{\partial x}\Big)\frac{\tilde{u}}{u_0} \tag{11}$$

where we have used the Mach number $Ma = u_0/c = qu_0/\omega$. The three real terms can then be neglected since we have:

$$\begin{cases} \frac{1}{qu_0}\frac{\partial u_0}{\partial x} &\simeq \frac{\lambda}{\xi} \ll Ma^{-1} \\ \frac{1}{qn_0}\frac{\partial n_0}{\partial x} &\simeq \frac{\lambda}{\xi} \ll 1 \\ \frac{K}{qu_0} &\simeq \frac{KT_w}{Ma} \ll Ma^{-1} \end{cases} \tag{12}$$

In other words, the wavelength of the waves remain small in comparison to extent $\xi$ of the flowing region, and their period remains small in comparison to the time scale $K^{-1}$ associated with proliferation. Then, continuity implies:

$$\frac{\tilde{n}}{n_0} = \frac{\tilde{u}}{u_0}\Big(\frac{1}{Ma} - 1\Big)^{-1} \tag{13}$$

Since $\frac{1}{Ma} - 1 \simeq \frac{1}{Ma} \simeq 10$, this means that the (dimensionless) amplitude of the density waves is about ten times smaller than that of the velocity wave. If the amplitude in velocity is 50%, then the amplitude in density is only 5%, which is bellow our resolution.

### 7.2 General velocity equation

The equation on the velocity we use to predict the emergence of waves depends on the continuity equation and on the relation between velocity and density. The dependency on the velocity-density relation can be encompassed using the following definition:

$$n' \equiv \frac{\partial n}{\partial u} \tag{14}$$

Then, we can progressively transform the continuity equation into a general equation on the velocity:

$$\frac{\partial n}{\partial t} + \frac{\partial (un)}{\partial x} = Kn \tag{15}$$

$$n'\frac{\partial u}{\partial t} + n\frac{\partial u}{\partial x} + u\frac{\partial n}{\partial x} = Kn \tag{16}$$

$$n'\frac{\partial u}{\partial t} + n\frac{\partial u}{\partial x} + un'\frac{\partial u}{\partial x} = Kn \tag{17}$$

$$\frac{\partial u}{\partial t} + \Big(u + \frac{n}{n'}\Big)\frac{\partial u}{\partial x} = K\frac{n}{n'} \tag{18}$$

The derivative of the density with respect to the velocity can then be expressed in terms of the mean cell radius, since $n = 1/(\pi R^2)$:

$$n' = \frac{\partial n}{\partial u} = \frac{\partial n}{\partial R}\frac{\partial R}{\partial u} = -\frac{2}{\pi R^3}\frac{\partial R}{\partial u} \tag{19}$$

The continuity equation reaches:

$$\frac{\partial u}{\partial t} + \Big(u - f(u)\Big)\frac{\partial u}{\partial x} = -Kf(u) \tag{20}$$

With:

$$f(u) \equiv \frac{R}{2}\frac{\partial u}{\partial R} \tag{21}$$

Introducing a harmonic perturbation, $u = u_0 + \tilde{u}$, with $\tilde{u} \ll u_0$, the function $f(u)$ can be expanded around $u_0$, in powers of $\tilde{u}$:

$$f(u) = f(u_0) + \frac{\partial f}{\partial u}\Big|_{u_0} \tilde{u} + \mathcal{O}(\tilde{u}^2) \tag{22}$$

The equation of the velocity linearised in the perturbation can then be expressed using $\tilde{f}(u_0) \equiv \frac{\partial f}{\partial u}\Big|_{u_0}$:

$$-i\omega + iq(u_0 - f(u_0)) = -K\tilde{f} - (1-\tilde{f})\frac{\partial u_0}{\partial x} \tag{23}$$

The generalized wave speed can then be expressed as:

$$c(u_0) = \omega_r/q = u_0 - f(u_0) \tag{24}$$

And the generalized growth rate of the instability is:

$$\omega_i = -K\tilde{f} - (1-\tilde{f})\frac{\partial u_0}{\partial x} \tag{25}$$

Let us now study the explicit form of these general equations for a few choices of velocity-density relations.

### 7.3 Piecewise velocity-radius relation

For the piecewise velocity-radius relation, the function $f(u)$ has two possible values:

$$\begin{cases} f(u) = \frac{u+u_r}{2} & \text{if } R_j < R < R_c \\ f(u) = 0 & \text{otherwise} \end{cases} \tag{26}$$

Thus, the general velocity equation (Eq. 20) can be expressed explicitly in the three domains:

$$\begin{cases} \frac{\partial u}{\partial t} + \frac{u-u_r}{2}\frac{\partial u}{\partial x} = -\frac{K}{2}(u+u_r) & \text{if } R_j < R < R_c \\ \frac{\partial u}{\partial t} + u\frac{\partial u}{\partial x} = 0 & \text{otherwise} \end{cases} \tag{27}$$

For the middle domain ($R_j < R < R_c$), we discussed the stability analysis in the article, where we found:

$$\begin{cases} \omega_r = \frac{u_0-u_r}{2} q \\ \omega_i = -\frac{1}{2}\left(K + \frac{\partial u_0}{\partial x}\right) \end{cases} \tag{28}$$

In the two other domains, the equation of the velocity is identical to the inviscid Burger equation, which is known to develop shocks.

### 7.4 Hyperbolic tangent velocity-radius relation

In the hyperbolic tangent model, we have:

$$f(u) = \frac{u(u_m - u)}{\Delta u_m}\left(R_0 + \Delta \tanh^{-1}\left(\frac{2u}{u_m} - 1\right)\right) \tag{29}$$

And:

$$\tilde{f} = \frac{1}{2} + \frac{u_m - 2u_0}{\Delta u_m}\left[R_0 + \Delta \tanh^{-1}\left(\frac{2u_0}{u_m} - 1\right)\right] \tag{30}$$

Note that the inverse hyperbolic tangent only has real solutions for arguments between $-1$ and 1, in other words if $u_0$ is in between 0 and $u_m$.

A connection can be made with the piecewise model, if $u = u_m/2 + \varepsilon$, with $\varepsilon \ll u_m$. Within this limit, the hyperbolic tangent reduces to a linear function. Then, we have:

$$f(u) \simeq \frac{u(u_m - u)}{u_m}\left(\frac{R_0}{\Delta} + \frac{2u - u_m}{u_m}\right) \tag{31}$$

$$\simeq \frac{u_m^2/4 - \varepsilon^2}{u_m}\left(\frac{R_0}{\Delta} + \frac{2\varepsilon}{u_m}\right) \tag{32}$$

$$\simeq \frac{u_m}{4}\left(\frac{R_0}{\Delta} - 1\right) + \frac{u}{2} + \mathcal{O}(\varepsilon^2) \tag{33}$$

$$\simeq \frac{u_r + u}{2} + \mathcal{O}(\varepsilon^2) \tag{34}$$

Where we used:

$$\begin{cases} \tau_v & \simeq \frac{2\Delta}{u_m} \\ R_j & \simeq R_0 - \Delta \\ R_c & \simeq R_0 + \Delta \end{cases} \tag{35}$$

Note that this model also underestimates the wave velocity.

### 7.5 Greenshields relation

For $R > R_j$, the Greenshields relation gives:

$$f(u) = u_m - u \tag{36}$$

And:

$$\tilde{f} = -1 \tag{37}$$

Thus, the predicted wave speed is:

$$c(u_0) = 2u_0 - u_m \tag{38}$$

And the generalized growth rate of the instability is:

$$\omega_i = K - 2\frac{\partial u_0}{\partial x} \tag{39}$$

Consequently, in this model of the velocity-density relation, the waves propagate forward rather than backward, since if we take the front speed for $u_0$ we have $2u_0 > u_m$. Besides, the proliferating case is actually more unstable, since the stability criterion is $K > 2\frac{\partial u_0}{\partial x}$. This does not reflect the trend observed in experiments.

# 8 Theory: Mechanical approach

## 8.1 Johnson-Segalman model

We consider a Maxwellian viscoelastic model of the stress:

$$\boldsymbol{\Sigma} = 2\eta \boldsymbol{D} - \tau_e \overset{\triangledown}{\boldsymbol{\Sigma}} \tag{40}$$

where $\eta$ is the viscosity, $\tau_e$ is the relaxation time, and where the material derivative is the so-called Gordon-Schowalter derivative with slip parameter $a$:

$$\overset{\triangledown}{\boldsymbol{\Sigma}} = \frac{D\boldsymbol{\Sigma}}{Dt} - (\boldsymbol{\Omega}\cdot\boldsymbol{\Sigma} - \boldsymbol{\Sigma}\cdot\boldsymbol{\Omega}) - a(\boldsymbol{D}\cdot\boldsymbol{\Sigma} + \boldsymbol{\Sigma}\cdot\boldsymbol{D}) \tag{41}$$

Since the flow is only along $x$, the convected derivative is just:

$$\frac{D\boldsymbol{\Sigma}}{Dt} = \frac{\partial \boldsymbol{\Sigma}}{\partial t} + u\frac{\partial \boldsymbol{\Sigma}}{\partial x} \tag{42}$$

For the flow under consideration, the symmetric part of the velocity gradient is:

$$\boldsymbol{D} = \frac{1}{2}(\nabla \boldsymbol{u}^\dagger + \nabla \boldsymbol{u}) = \frac{1}{2}\begin{pmatrix} 2\dot{\gamma}_x & 0 & \dot{\gamma}_z \\ 0 & 0 & 0 \\ \dot{\gamma}_z & 0 & 0 \end{pmatrix} \tag{43}$$

And the antisymmetric part is:

$$\boldsymbol{\Omega} = \frac{1}{2}(\nabla \boldsymbol{u}^\dagger - \nabla \boldsymbol{u}) = \frac{1}{2}\begin{pmatrix} 0 & 0 & \dot{\gamma}_z \\ 0 & 0 & 0 \\ -\dot{\gamma}_z & 0 & 0 \end{pmatrix} \tag{44}$$

For this flow, the components of the material derivative are:

$$\overset{\triangledown}{\Sigma}_{xx} = \frac{D\Sigma_{xx}}{Dt} - 2a\dot{\gamma}_x\Sigma_{xx} - (1+a)\dot{\gamma}_z\Sigma_{xz} \tag{45}$$

$$\overset{\triangledown}{\Sigma}_{xz} = \frac{D\Sigma_{xz}}{Dt} - a\dot{\gamma}_x\Sigma_{xz} + \frac{1-a}{2}\dot{\gamma}_z\Sigma_{xx} \tag{46}$$

## 8.2 Development in powers of $\tau_e$

The convective derivative provide corrections of order $\tau_e$ and above to the long time viscous response, which are of order $\tau_e^0$:

$$\Sigma_{xx} = 2\eta\dot{\gamma}_x + \mathscr{O}(\tau_e) \tag{47}$$

$$\Sigma_{xz} = \eta\dot{\gamma}_z + \mathscr{O}(\tau_e) \tag{48}$$

Replacing every instance of $\Sigma_{xx}$ and $\Sigma_{xz}$ by their leading order term in the expressions of the components material derivative, we get:

$$\overset{\triangledown}{\Sigma}_{xx} = 2\eta\frac{D\dot{\gamma}_x}{Dt} - 4a\eta\dot{\gamma}_x^2 - (1+a)\eta\dot{\gamma}_z^2 + \mathscr{O}(\tau_e) \tag{49}$$

$$\overset{\triangledown}{\Sigma}_{xz} = \eta\frac{D\dot{\gamma}_z}{Dt} + (1-2a)\eta\dot{\gamma}_z\dot{\gamma}_x + \mathscr{O}(\tau_e) \tag{50}$$

Then, if we only keep terms up to order $\tau_e^1$, we can refine our approximation of the stress components:

$$\Sigma_{xx} = 2\eta\dot{\gamma}_x - 2\eta\tau_e\frac{D\dot{\gamma}_x}{Dt} + 4a\eta\tau_e\dot{\gamma}_x^2 + (1+a)\eta\tau_e\dot{\gamma}_z^2 + \mathscr{O}(\tau_e^2) \tag{51}$$

$$\Sigma_{xz} = \eta\dot{\gamma}_z - \eta\tau_e\frac{D\dot{\gamma}_z}{Dt} - (1-2a)\eta\tau_e\dot{\gamma}_z\dot{\gamma}_x + \mathscr{O}(\tau_e^2) \tag{52}$$

Moving to the stress gradients we get:

$$\frac{\partial\Sigma_{xx}}{\partial x} = -2\eta\tau_e\frac{\partial^3 u}{\partial t\partial x^2} - 2\eta\tau_e u\frac{\partial^3 u}{\partial x^3} + 2(1+a)\eta\tau_e\frac{\partial u}{\partial z}\frac{\partial^2 u}{\partial x\partial z} \tag{53}$$

$$+ 2\eta\left(1 + (4a-1)\tau_e\frac{\partial u}{\partial x}\right)\frac{\partial^2 u}{\partial x^2} + \mathscr{O}(\tau_e^2) \tag{54}$$

$$\frac{\partial\Sigma_{xz}}{\partial z} = -\eta\tau_e\frac{\partial^3 u}{\partial t\partial z^2} - \eta\tau_e u\frac{\partial^3 u}{\partial x\partial z^2} - 2(1-a)\eta\tau_e\frac{\partial u}{\partial z}\frac{\partial^2 u}{\partial x\partial z} \tag{55}$$

$$+ \eta\left(1 - (1-2a)\tau_e\frac{\partial u}{\partial x}\right)\frac{\partial^2 u}{\partial z^2} + \mathscr{O}(\tau_e^2) \tag{56}$$

Enforcing the lubrication approximation, we keep terms in $1/z^2$:

$$\frac{\partial \Sigma_{xx}}{\partial x} \simeq 2(1+a)\eta\tau_e \frac{\partial u}{\partial z}\frac{\partial^2 u}{\partial x \partial z} \tag{57}$$

$$\frac{\partial \Sigma_{xz}}{\partial z} \simeq -\eta\tau_e \frac{\partial^3 u}{\partial t \partial z^2} - \eta\tau_e u \frac{\partial^3 u}{\partial x \partial z^2} - 2(1-a)\eta\tau_e \frac{\partial u}{\partial z}\frac{\partial^2 u}{\partial x \partial z} \tag{58}$$

$$+\eta\Big(1-(1-2a)\tau_e\frac{\partial u}{\partial x}\Big)\frac{\partial^2 u}{\partial z^2} \tag{59}$$

Note that the lubrication approximation selects a term of order $\tau_e^1$, rather than $\tau_e^0$, as the leading term for the normal stress. Then, the force balance is:

$$u\frac{\partial^3 u}{\partial x \partial z^2} + \frac{\partial^3 u}{\partial t \partial z^2} = 4a\frac{\partial u}{\partial z}\frac{\partial^2 u}{\partial x \partial z} + \frac{\partial^2 u}{\partial z^2}\Big(\frac{1}{\tau_e} - (1-2a)\frac{\partial u}{\partial x}\Big) \tag{60}$$

## 8.3 Refining the approximations of the gradients

### 8.3.1 Simplest approximation

In the article, we have seen that if we assume that $\partial/\partial z = 1/h$, with $h$ constant, then the force balance becomes:

$$\frac{\partial u}{\partial t} + 2(1-3a)u\frac{\partial u}{\partial x} = \frac{u}{\tau_e} \tag{61}$$

This equation is close to the one we obtained in the kinematic approach, but it is not exactly the same. From the two sides of the equation we can gather that:

$$f(u) = u(6a-1) \tag{62}$$

$$f(u) = -\frac{1}{K\tau_e}u \tag{63}$$

The first equation for $f(u)$ implies the following velocity-radius relation:

$$u(R) = \phi R^{2(6a-1)} \tag{64}$$

where $\phi$ is a constant. Note that such velocity-radius relation does not fit our experimental data, crucially because it lacks the threshold associated with the fact that for $R < R_j$ we have $u \simeq 0$.

Equating the two expressions for $f(u)$ implies the following relation between the viscoelastic time and the proliferation rate:

$$K\tau_e = (1-6a)^{-1} \tag{65}$$

This equation suggests that proliferation has an impact on the value of the slip parameter as discussed in the article. Indeed, since we always have $\tau_e > 0$, this implies that $K > 0$ if and only if $a < 1/6$. Nevertheless, such inequality would also lead to a velocity-radius relation where the velocity decreases with increasing radius, which is not observed in experiments.

### 8.3.2 Adding a constant shear

To refine our approximation of the gradients in Eq. 60 and come closer to the velocity equation obtained in the kinematic approach, we can add a constant shear:

$$\frac{\partial u}{\partial z} = \dot{\gamma}_0 + \frac{u}{h} \tag{66}$$

$$\frac{\partial^2 u}{\partial z^2} = \frac{\dot{\gamma}_0}{h} + \frac{u}{h^2} \tag{67}$$

Then, the force balance is:

$$\frac{\partial u}{\partial t} + 2(1-3a)u\frac{\partial u}{\partial x} + \dot{\gamma}_0 h(1-6a)\frac{\partial u}{\partial x} = \frac{u}{\tau_e} + \frac{\dot{\gamma}_0 h}{\tau_e} \tag{68}$$

From the two sides of the equation we can gather:

$$f(u) = (6a-1)(u+\dot{\gamma}_0 h) \tag{69}$$

$$f(u) = -\frac{1}{K\tau_e}(u+\dot{\gamma}_0 h) \tag{70}$$

Equating the two equations leads to the same relation between $K\tau_e$ and $a$ that we found in the previous sub-section. On the other hand, the first equation for $f(u)$ implies a different velocity-radius relation, including a shift:

$$u(R) = \phi R^{2(6a-1)} - \dot{\gamma}_0 h \tag{71}$$

Comparing this equation with the linear relation we used in the kinematic approach, this suggests the following identities:

$$\begin{cases} a &= \frac{1}{4} \\ K &= -\frac{2}{\tau_e} \\ c &= \frac{u_0}{2} \\ u_r &= \dot{\gamma}_0 h \end{cases} \tag{72}$$

Such value of $a$ necessarily corresponds to a case without cell divisions ($K < 0$), even though we found that both proliferating and non-proliferating conditions share the same form of velocity-radius relation, and so the same form of equation on the velocity. Moreover, the predicted wave speed $c$ is positive instead of being negative. These discrepancies between the kinematic and mechanical approaches cannot be resolved by the addition of a constant shear.

## 9 Movie.

The movie shows two representative examples of epithelial dynamics with (top) or without (bottom) proliferation, in stripes of width $200\mu$m. The movies display an overlay of the phase contrast images and the intensity of the velocity field along the stripe length ($x$) computed with PIV. The color code extend from null (blue) to speeds of $1\mu$m/min (red). Time is given in hours.